J Mater Sci (2007) 42:1261–1268
DOI 10.1007/s10853-006-1145-x

Elastic properties of powders during compaction. Part 1: Pseudo-isotropic moduli

M. L. Hentschel · N. W. Page

Received: 20 May 2004 / Accepted: 13 January 2006 / Published online: 22 November 2006

Abstract The elastic moduli of powdered materials undergoing uniaxial compaction was investigated, paying particular attention to effects of solid phase material properties and initial particle shape. Elastic properties were characterised by the isotropic elastic moduli Poisson's ratio and Young's modulus, calculated from elastic wave speeds measured in the axial (pressing direction). To isolate material property effects, three different ductile metal powders (copper, stainless steel, and aluminium) with equivalent particle shape (spheroidal) were tested. Comparison with similar measurements for a brittle spheroidal powder (glass) illustrated that solid phase yield mechanism affects the evolution of pore character, and hence bulk elastic properties of the powder compact. Pore character was also studied separately by comparing copper powders with differing particle shapes (spheroidal, irregular, and dendritic).

For all powders, Young's modulus increased monotonically with compaction (reducing porosity). For the ductile spheroidal powders, differences in evolution of Young's modulus with compaction were accounted for by solid phase elastic properties. The different morphology copper powders showed an increase in compact compliance as particle (pore) ruggedness increased. Poisson's ratio followed a concave porosity dependence: decreasing in the initial stages of compaction, then increasing as porosity approached zero. Comparison between powders indicated the initial decrease in Poisson's ratio was insensitive to solid phase material properties. However, as the compact approached solid phase density, the Poisson's ratio—porosity locus diverged towards corresponding solid phase values for each particle material, indicating an influence of solid phase elastic properties.

M. L. Hentschel
Mechanical Engineering, The University of Newcastle, Newcastle, NSW 2308, Australia

N. W. Page (✉)
141 Long St East, Graceville, Qld 4075, Australia
e-mail: npage2@telstra.com

Introduction

Elastic behaviour of powdered materials has implications for seismological events, foundations engineering, crushing operations, powder metallurgy, tableting of pharmaceutical powders, particle size enlargement processes, and discharge of bulk solids from storage facilities, etc. This work considers the elastic moduli of a powder undergoing uniaxial compaction, giving specific consideration to the influence of particle material properties and particle shape. Elastic moduli were calculated from in-situ elastic wave speed measurements, as common quasi-static testing methods (compression, tensile, bend tests, etc.) are not appropriate for powdered materials [1–5].

Complete elastic characterisation of an isotropic, linear elastic, homogeneous body requires at least two elastic moduli. In this work, Young's modulus (E) and Poisson's ratio (v) are used for this purpose. Effects of solid phase material properties and pore character can be inferred from literature on elastic properties of porous materials, and some limited results on elastic moduli measured in-situ [6–15]. Taken as a whole, the body of literature indicates the following effects of

sample microstructure. Total porosity affects both E [1, 3, 16–26] and ν [9, 17, 19–21, 23–25, 27–29]. ν appears less sensitive to porosity; though the greater difficulties in obtaining a precise measurement of ν may contribute. Pore character also has an effect. Analysis has shown at least two attributes influence the elastic response: increasingly elongate and irregular pores both reduce stiffness [30, 31], with spherical pores providing the stiffest possible system for a given porosity [31]. Interaction between adjacent pores is also important, as this modifies surrounding mechanical fields [16, 18, 32]. Interconnection of previously isolated pores is the limiting case of pore interaction, and is important in practice because extensive interconnection precludes use of the familiar concept of shape to describe pore character [24, 28, 33–35]. Solid phase elastic properties affect E over a large range of porosity [16, 17]; likewise ν [17, 36]. The influence of solid phase properties appears to reduce at high porosities, presumably when the response is dominated by contact geometry (pore character). Solid phase (inter-particle) bonding is also important, with increases in bond strength (e.g. by sintering) resulting in a stiffer structure [21, 26, 37–39]. Finally, any interstitial fluid may also have an influence; however, for air-saturated powders the disparity between solid and gaseous phase properties renders this negligible.

Several recurring themes emerge from the literature. Firstly, most work concentrates on a single elastic property, overwhelmingly E. Very few results are available on the effects of sample microstructure on ν. Many studies consider only a single material type, and a narrow porosity range. Thus, it is difficult to evaluate generality of results obtained. Also common amongst published experimental data is the lack of material characterisation for variables other than the one being investigated. This appears due, in part, to the variables chosen for study. Many studies have a quality control emphasis, focussing on variables more descriptive of sample processing rather than sample state (microstructure); an approach which neglects the link between sample properties and microstructure. When a specific microstructural variable is considered, usually little effort is made to ensure other microstructural features remain constant. Thus, observed variations in the elastic behaviour attributed to one variable (e.g. particle size) may be confounded by corresponding changes in another (e.g. particle shape). This study seeks to address these issues by comparing a number of different powders selected to isolate, as best possible, the influence of a single microstructural feature on elastic properties. Uniaxial compaction was adopted to provide access to a wide porosity range, while elastic wave speed measurements ensures true elastic properties are measured.

Experimental

Eight different powders, covering a variety of solid phase materials and particle shapes were studied (see Table 1, Fig. 1). All powders were sieved, selecting the size fraction +75-106 μm to minimise effects of particle size differences.

As an initial step towards description of pore structure, shape of undeformed powder particles was quantified by use of the descriptors aspect ratio (AR = *ratio of minimum to maximum Feret diameters*), and the square root of form factor ($\sqrt{\text{FF}} = 2(\pi \text{ area})^{1/2}/\text{perimeter}$); median values are listed in Table 1. These descriptors have been found to be useful for characterising particle elongation, and boundary irregularity (ruggedness) respectively [40]. As discussed previously, both shape attributes affect elastic behaviour. Significant particle shape differences are evident between the copper powders. The spheroidal powder (D) is smooth and compact while the irregular powders (B, C) and the dendritic powder (A) have an increasingly rugged appearance and are slightly more elongate. As these three powders have the same solid phase elastic properties and yield behaviour, comparison allows effects of pore character to be evaluated. By contrast, the three spheroidal metal powders (D, E, F) can be used to evaluate effects of solid phase elastic properties on the bulk elastic response. As particle shape is closely matched, the initial pore structure will be equivalent. Importantly, all are ductile metal powders with similar yield behaviour (predominately plastic flow), and thus, pore character will evolve in a similar fashion. This allows comparison of solid phase elastic properties over a wide porosity range. For the spheroidal glass powder (G), the dominant yield mechanism is brittle fracture. Hence, though initially similar, pore character within the glass compact will diverge from the spheroidal ductile metal powders during compaction, allowing the effect of yield mechanism to be evaluated. The irregular copper powders (B, C) and the irregular iron powder (H) also have similar particle shape, and thus, comparison ensures results on the effect of solid phase material properties are not specific to spheroidal powders.

Powders were uniaxially compacted in a rigid cylindrical die using applied pressures up to a maximum of 560 MPa. Ultrasonic transducers within the die assembly allowed for in-situ measurement of shear and longitudinal elastic wave speeds in the axial (pressing)

Table 1 Powder details

Powder	Particle shape[a]	Source	Manufacturers Designation	Porosity of gravity-induced packings[b]		Shape descriptors	
				p_a	p_{tap}	AR	√FF
A. Dendritic copper	Dendritic	Electrolytic deposition, MicroMet, Hamburg, Germany.	Grade M	0.7374 (±0.0013)	0.692 (±0.004)	0.605	0.796
B. Irregular copper (MM)	Irregular	Water atomization process, MicroMet, Hamburg, Germany.	Irregular - 160 μm	0.6492 (±0.0008)	0.583 (±0.005)	0.717	0.822
C. Irregular copper (US)	Irregular	Water atomization process, U.S. Bronze Powders, Flemington USA.	US180	0.717 (±0.001)	0.650 (±0.005)	0.723	0.839
D. Spheroidal copper	Spheroidal	Gas atomization process, Makin Metal Powders, Lancashire, England.	SCP 60#	0.423 (±0.008)	0.370 (±0.027)	0.934	0.994
E. Stainless steel	Spheroidal	Gas atomization process, Anval Nyby Powder, Torshalla, Sweden.	316L	0.469 (±0.013)	0.379 (±0.026)	0.843	0.957
F. Aluminium	Spheroidal	Gas atomization process, Alloys International, Melbourne, Australia.	1020	0.5141 (±0.0015)	0.40 (±0.01)	0.773	0.931
G. Glass	Spheroidal	Potters Industries Laverton, Vic. Australia.	Glass ballotini	0.448 (±0.009)	0.365 (±0.009)	0.943	0.990
H. Iron	Irregular	Nilsen Sintered Products Melbourne, Australia.	Höganäs NC100.24	0.6977 (±0.0004)	0.625 (±0.005)	0.718	0.855

[a] Terminology of British Standard 5600

[b] p_a is the porosity of the apparent density state, while p_{tap} corresponds to the tap density state. These measurements were performed as codified in ASTM B212, and B527. Bracketed numbers denote measurement uncertainty

direction throughout compaction, and hence elastic moduli of the compact to be calculated [41] as a function of porosity. Results in this paper are presented in terms of the isotropic moduli Young's modulus (E) and Poisson's ratio (ν). A companion paper [42] reports on compaction-induced elastic anisotropy inferred from additional wave speed measurements in the radial direction. Significant deviations from isotropy do occur [42]; however, the moduli derived from axial wave speed measurements are found to be indicative of analogous elastic moduli for the axial plane [42]. For this reason elastic moduli presented here are denoted 'pseudo-isotropic'. Further details on experimental methods and powder characterisation have been presented elsewhere [43].

Results and discussion

Solid phase material effects

Effects of solid phase elastic properties are determined from the elastic moduli presented in Figs. 2 and 3 as a function of compact porosity. Normalised Young's modulus is seen to increase monotonically as porosity is reduced; consistent with an expected increase in stiffness as the compact is densified. Poisson's ratio has a concave dependence: initially decreasing as porosity is reduced, before increasing to approach the solid phase value as porosity approaches zero. These results for E and ν follow the same qualitative pattern of an earlier study [17] which used mechanical testing to deduce elastic moduli. However, in that previous work, E was up to 30% lower than reported here, especially so at low porosity. Poisson's ratio was also qualitatively similar, but quantitatively ν was significantly lower in the earlier work than found here. These differences are attributed to the measurement techniques used. Previously [17], elastic moduli were determined from intermittent periods of unloading during compaction. This, and other quasi-static testing methods, requires the unloading response to be purely elastic: an assumption which is not justified [1–4]. Measurement of true elastic properties is best performed by elastic wave speed measurements [5], as adopted here.

Figure 2a indicates that normalising by solid phase Young's modulus brings results for the three different spheroidal metal powders into close coincidence throughout compaction. In contrast, while E/E_{solid} for the brittle spheroidal glass powder is initially similar to the ductile spheroidal metal powders, it quickly diverges as porosity is reduced. This is attributed to differences in the evolution of pore character which, in turn, result from differences in solid phase yield mechanism, i.e. fracture compared to plastic flow. Hence, E_{solid} accounts for differences in $E(p)$ provided the initial pore character is similar and pore character evolves in the same manner during compaction. Effects of normalisation

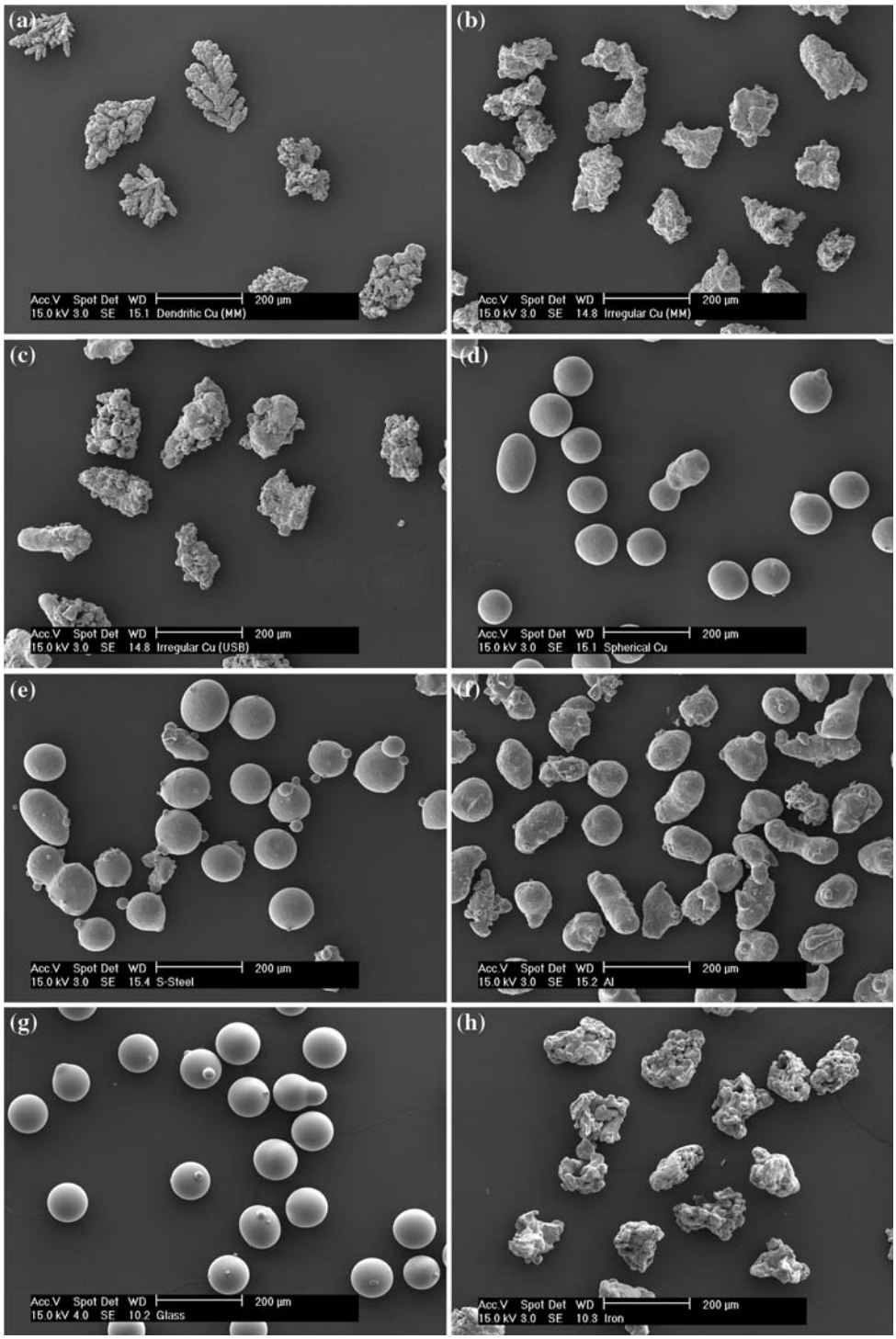

Fig. 1 Scanning electron micrographs of the powders, illustrating particle shape. (a) Dendritic copper, (b) Irregular copper (MM), (c) Irregular copper (US), (d) Spheroidal copper, (e) Stainless steel, (f) Aluminium, (g) Glass, (h) Iron

are not confined to spheroidal powders. Both irregular copper powders, and the iron powder also have similar particle shape (Table 1, Figs. 1b, c, h), and solid phase Young's modulus again brings $E(p)$ into close coincidence for both materials (Fig. 3a).

In contrast, Fig. 2b indicates the evolution of Poisson's ratio in the initial stages of compaction is not affected by solid phase material properties (Table 2). Instead, $v(p)$ appears to initially be dominated by differences in pore character (particle shape). However, this insensitivity to solid phase properties cannot hold throughout: eventually, v for the stainless steel powder must diverge from the spheroidal aluminium and copper powders to approach its solid phase value

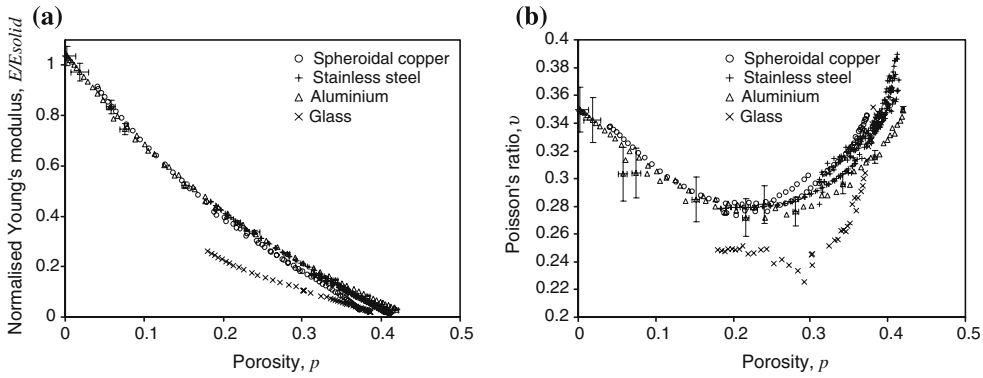

Fig. 2 Effect of particle material on elastic moduli of spheroidal powders during compaction. (○) Spheroidal copper; (+) Stainless steel; (Δ) Aluminium; (×) Glass. (a) Young's modulus normalised by E_{solid}, (b) Poisson's ratio

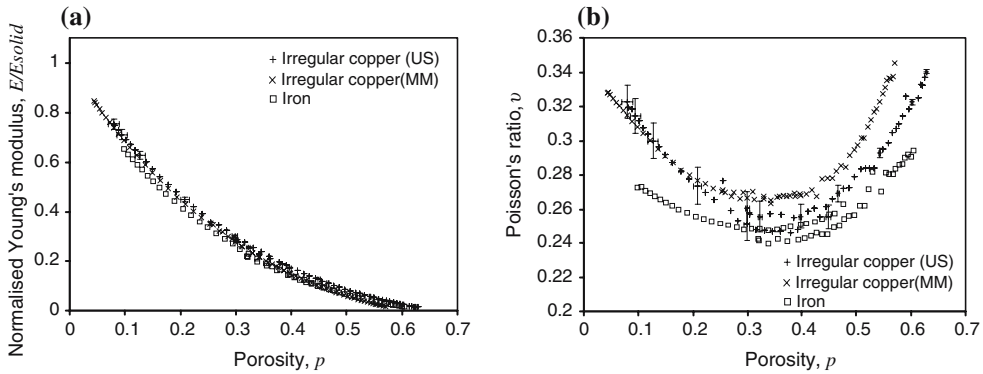

Fig. 3 Effect of particle material on elastic moduli of irregular powders during compaction. (+) Irregular copper (US); (×) Irregular copper (MM); (□) Iron. (a) Normalised Young's modulus, (b) Poisson's ratio

Table 2 Solid phase material properties

Material	Density, ρ_{solid}, (kg m^{-3})	Young's modulus, E_{solid}, (GPa)	Poisson's ratio, ν_{solid}, (–)
Copper [44]	8960	115	0.35
Stainless steel [45]	8000	195	0.29
Aluminium [46]	2700	67.6	0.35
Glass [47]	2450	64	0.244
Iron [46]	7690	203	0.29

(0.29) as porosity reduces to zero. Due to the relative difficulty of compacting stainless steel powder to lower porosities, data to evaluate this expected divergence is not available. Further pursuit of this point relies on comparison of the irregular iron and copper powders, which also have similar particle shapes. Figure 3b shows that $\nu(p)$ again follows a concave path during compaction, similar to the spheroidal powders (Fig. 2b). Agreement in the initial stages of compaction is not as strong as for the spheroidal powders; this is attributed to minor particle shape differences as it is noticeable ν differs in the same order as the measured particle irregularity ($\sqrt{FF}$ in Table 1). Significantly though, $\nu(p)$ for the irregular copper powders come into closer agreement as they asymptote towards ν_{solid} in the final stages of compaction. In this same low-porosity region, $\nu(p)$ for the iron powder diverges to approach the solid phase value for iron. Together the data for spheroidal and irregular powders suggest $\nu(p)$ at high porosity is attributable mainly to pore character and is relatively insensitive to solid phase material properties, but at low porosities, ν_{solid} assumes increasing importance for determining $\nu(p)$. Given these act in a different sense, the intermediate porosity range where Poisson's ratio is approximately constant is attributed to a transition region where the effects balance. While the influence of ν_{solid} on $\nu(p)$ as the compact approaches solid phase density is straightforward, insensitivity of $\nu(p)$ to ν_{solid} at high porosity is less so. It is suggested this is a consequence of the bulk elastic response being dominated by the compliance of the interparticle contact region in the initial stages of compaction. Initially contact areas are relatively small and well separated, hence localised Poisson effects (i.e. lateral strain resulting from a local normal strain) have a greater probability of intruding into pore space. Local lateral deformation 'absorbed' by pores (rather than straining adjacent solid phase material and transferring deformation throughout the bulk), would serve to suppress effects of solid phase Poisson's ratio, with pore character effects dominating instead. Reduction in porosity would then have a two-fold effect: firstly the amount of pore space available to 'absorb' local lateral deformation is reduced; and secondly, the

increasing contact size (by permanent solid phase deformation) would reduce the dominance of the interparticle contact region, with increasingly more of the solid phase material becoming involved in transfer of elastic strain. Improved structural interconnections would increase the efficiency with which lateral elastic deformation is transferred throughout the bulk, and, as this occurs the solid phase elastic properties must assume an increasingly dominant role.

Pore character (particle shape) effects

The influence of pore character was studied by comparing elastic moduli of copper powders with different shaped particles (spheroidal, irregular, dendritic). As particle shape profoundly affects the porosity of the initial packing (Table 1), elastic moduli for these powders are compared on the basis of the compact *densification parameter*, D^* (Eq. 1), rather than porosity. This takes some account of the differences in the amount of solid phase deformation (bonding) which exists on a porosity basis. For instance, whereas the dendritic and irregular powders required applied pressures of 50–60 MPa to reduce the total porosity to 0.42, this is possible under gravitational loading for the spheroidal powder. Clearly, this would produce significant differences in interparticle bonding (by particle interlocking, etc.), and hence, the ability to transfer deformation throughout the bulk would be quite different for the different shaped powders.

$$D* = \frac{p_a - p}{p_a} \tag{1}$$

p is porosity and p_a is the porosity of the apparent density state (see Table 1).

Results for E and ν (Fig. 4) show that for all particle shapes, each elastic modulus converges towards the solid phase value for copper as the compact approaches solid density. Thus, initial differences in pore character diminish as porosity is reduced towards zero. As complete densification is approached, pores become increasingly equi-axed (spheroidal) in nature, and the different loci converge. The spheroidal powder has the most distinct locus, reflecting shape characterisation results for the unpressed powders (Table 1).

$E(D^*)$ for the irregular and dendritic powders is highly non-linear throughout compaction, in contrast to the spheroidal powder, for which $E(D^*)$ remains approximately linear throughout. This difference is suggested to be due to differences in boundary irregularity between the powders. While the spheroidal particles are relatively smooth, both irregular and dendrite powders are characterised by many surface protuberances (asperities). In initial stages of compaction, the size of interparticle contacts will be significantly smaller, and hence more compliant for the more rugged powders. The dendritic powder has a further consideration, as the dendrite arms can also undergo elastic deformation by bending, further increasing the compliance of the dendritic powder relative to the irregular powders.

By virtue of high localised stresses at contacting surface protuberances, solid phase yield will also initiate at these points. For a ductile material, plastic flow will act to flatten contacts and increase their area as compaction proceeds, until contact occurs between the convex hulls of the particles. After this point, contact area will increase rapidly, and correspondingly, compact stiffness will increase at a greater rate. At the macroscopic level, this corresponds to a faster increase in Young's modulus with densification. In contrast, for the spheroidal powder, the same contact geometry of two initially spherical surfaces with a flattened contact region will prevail throughout and hence the rate at

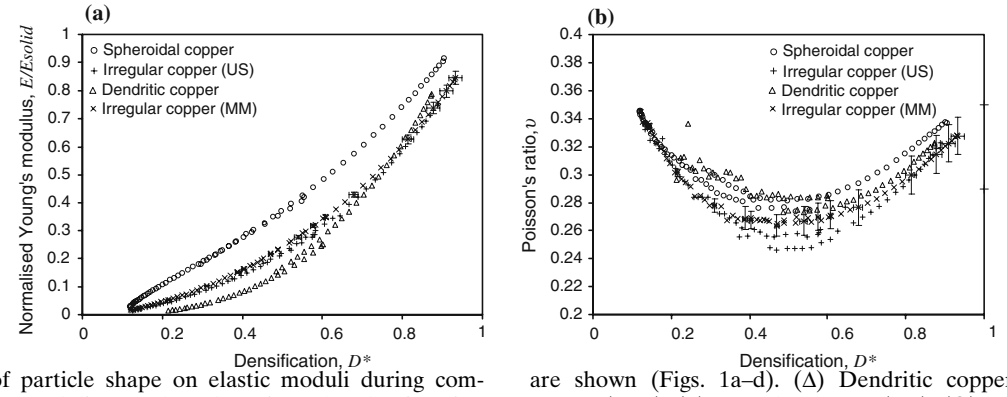

Fig. 4 Effect of particle shape on elastic moduli during compaction. Elastic moduli are plotted against the densification parameter, D^*, (Eq. 1). Data for four different copper powders are shown (Figs. 1a–d). (Δ) Dendritic copper; (×) Irregular copper (MM); (+) Irregular copper (US); (○) Spheroidal copper (□). (a) Normalised Young's modulus. (b) Poisson's ratio

which E increases remains relatively constant. Nonlinearities may be expected at high porosities due to particle 'bridging' and minor irregularities (such as those evident on some stainless steel and aluminium particles used in this work); likewise, strain hardening of the deformed solid phase material at particle contacts may also increase the rate of stiffening at low porosities. It is emphasised however, that this phenomenological description applies to a ductile powder for which plastic flow will generally increase contact area: contact geometry in a brittle powder is expected to evolve differently, as solid phase yield will produce sharp, angular fracture debris.

Effective Poisson's ratio for the different copper powders again follows a concave dependence during densification. For both spheroidal and irregular particles $v(D^*)$ is very similar for $D^* \leq 0.2$, after which v for the irregular powder diverges towards lower values. The good agreement between the spheroidal and dendritic powders at low D^* (Fig. 4b) suggests that, in contrast to the case for effective Young's modulus, localised deformation of protuberances is not the controlling mechanism for the dependence of Poisson's ratio in this range of D^*.

Conclusions

Measurement of ultrasonic wave speeds during uniaxial compaction of powders has allowed calculation of instantaneous elastic properties during the compaction process. These have been analysed to show the effects of solid phase elastic properties, solid phase yield mechanism, and pore character through the initial particle shape.

For all powders, Young's modulus increased monotonically towards its solid phase value as porosity decreased towards zero. Normalisation by solid phase Young's modulus accounted for differences between materials with equivalent pore character. Powders with different solid phase yield mechanism (ductile and brittle) produced a different porosity evolution as the inter-particle contact geometry, and hence pore character, evolved in a different manner. Particle shape affected the evolution of Young's modulus. At high porosity, powders with low values of aspect ratio and form factor were more compliant, but there was some convergence in stiffness as porosity decreased.

For all powers Poisson's ratio initially decreased with decreasing porosity. This section of the porosity evolution was insensitive to solid phase elastic properties, being linked instead to the pore character. Approximately mid-way through compaction, the solid phase properties began to exert influence, causing the porosity evolution of v to shift towards its solid phase value as porosity approached zero. Again, differences in particle shape and solid phase yield mechanism affected the evolution of Poisson's ratio with porosity. Powder particle shape had the larger effect with powders with lower aspect ratio and form factor having lower values than the more spherical powders.

Both Young's modulus and Poisson's ratio were higher than values obtained in previous work [17] in which the elastic moduli were deduced from mechanical tests on the powders. This suggests that the deformation observed in the earlier work was not truly elastic.

Acknowledgement The authors gratefully acknowledge scholarship support for MLH through the Australian Research Council Small Grants Scheme.

References

1. Leheup ER, Moon JR (1980) Powder Metal 23:15
2. Straffelini G, Fontanari V, Molinari A (1999) Mater Sci Eng A 260:197
3. Moon JR (1989) Powder Metall 32:132
4. Sawicki A, Swidzinski W (1998) Powder Technol 96:24
5. Hardin BO, Blandford GE (1989) J, Geotech Engng 115:788
6. Jones MP, Blessing GV (1988) In: McGonnagle WJ (ed) International advances in nondestructive testing, vol 13. Gordon and Breach, New York, p 175
7. Kathrina T, Rawlings RD (1997) J Eur Ceram Soc 17:1157
8. ALeR Dawson L. Piché, Hamel A (1996) Powder Metall 39:275
9. Jones MP, Blessing GV (1987) In: Proceedings of 1987 IEEE ultrasonics symposium. 1186:587
10. Kendall K (1990) Br Ceram Trans 89:211
11. Brettell JM (1989) J Aust Phys 42:627
12. Brettell JM (1994) J Acoust Soc Am 95:2281
13. Jones MP, Blessing GV (1986) Nondestructive Testing Commun 2:155
14. Kathrina T, Rawlings RD (1996) Br Ceram Trans 95:233
15. ALeR Dawson, Pelletier S, Bussiére J (1996) Adv Powder Metall Particulate Mater 2:303
16. Rice W (1998) Porosity of ceramics. Marcel Dekker New York
17. Carnavas PC, Page NW (1998) J Mater Sci 33:4647
18. Luo J, Stevens R (1999) Ceram Int 25:281
19. Dean EA (1983) J Am Ceram Soc 66:847
20. Martin LP, Dadon D, Rosen M (1996) J Am Ceram Soc 79:1281
21. Green DJ, Nader C, Brezny R (1990) In: Handwerker CA, Blendell JE, Keyser W (eds) Ceramic transactions, vol. 7, Sintering of advanced ceramics. American Ceramic Society, Ohio
22. Nagarajan A (1971) J Appl Phys 42:3693
23. Chang L-S, Chuang T-H, Wei WJ (2000) Mater Charact 45:221
24. Asmani M, Kermel C, Leriche A, Ourak M (2001) J Eur Ceram Soc 21:1081

25. Adachi T, Sakka S (1990) J Mater Sci 25:4732
26. Cytermann R, Guyon E, Roux S (1988) Powder Metall Int 20:23
27. Ashkin D, Haber RA, Wachtman JB (1990) J Am Ceram Soc 73:3376
28. Haynes R, Egediege JT (1989) Powder Metall 32:47
29. Soga N, Schreiber E (1968) J Am Ceram Soc 51:465
30. Zimmerman RW (1985) J Appl Mech 52:606
31. Zimmerman RW (1986) J Appl Mech 53:500
32. Tsukrov I, Novak J (2002) Int J Solids Struct 39:1539
33. Rice RW (1976) J Am Ceram Soc 59:536
34. Rice RW (1997) J Mater Sci 32:1801
35. Boccaccini AR, Ondracek G, Mazilu P, Windelberg D (1993) J Mech Behav Mater 4:119
36. Boccaccini AR (1994) J Am Ceram, Soc 77:2779
37. Nanjangud SC, Brezny R, Green DJ (1995) J Am Ceram Soc 78:266
38. Patterson BR, Miljus KL, Knopp WV (1984) Powder Metal Report 39:145
39. Yeheskel O, Pinkas M, Dariel MP (2003) Mater Lett 57:4418
40. Hentschel ML, Page NW (2003) Part Part Syst Charact 20:25
41. Mason WP (1958) Physical acoustics and the properties of solids. Van Nostrand, New Jersey
42. Hentschel ML, Page NW, Elastic properties of powders during compaction. Part 2: Elastic anisotropy. Accepted for publication in J. Mater. Sci
43. Hentschel ML (2002) PhD Thesis, The University of Newcastle
44. Kalpakjian S (1985) Manufacturing processes for engineering materials. John Wiley and Sons, Chichester
45. Bever B (1986) Encyclopaedia of materials science and engineering. Plenum Press, New York
46. Drumheller DS (1998) Introduction to wave propagation in nonlinear fluids and solids. Cambridge University Press, Cambridge
47. Abdel -Ghani M, Petrie JG, Seville JPK, Clift R, Adams MJ (1991) Powder Technol 65:113